THESIS

IMPLICATIONS OF CELL COMPOSITION AND SIZE ON THE PERFORMANCE OF MICROALGAE ULTRASONIC HARVESTING

Submitted by

Alyssa Jean Aligata

Department of Mechanical Engineering

In partial fulfillment of the requirements

For the Degree of Master of Science

Colorado State University

Fort Collins, Colorado

Summer 2018

Master's Committee:

Advisor: Anthony Marchese
Co-Advisor: Jason Quinn

Christie Peebles

Copyright by Alyssa Jean Aligata 2018

All Rights Reserved

ABSTRACT

IMPLICATIONS OF CELL COMPOSITION AND SIZE ON THE PERFORMANCE OF MICROALGAE ULTRASONIC HARVESTING

Substantial economic challenges exist across the value chain for microalgae-based biofuels and bioproducts. Acoustic harvesting could dramatically reduce harvesting costs and directly address current energy barriers to separating algae from growth media. This technology utilizes ultrasonic standing waves to create an acoustic radiation force that, due to differences in the acoustic properties of the cells and media, causes the microalgae cells to agglomerate and settle out of the solution. The magnitude of the acoustic radiation force is directly related to the cell radius and acoustic contrast factor (ACF), the latter of which is a function of the density and compressibility of the cell. These properties can vary widely depending on the algae species, cultivation conditions, and growth stage—all of which affect the composition of the microalgae cells (e.g., lipid, carbohydrate, protein content). In this work, two methods were used to determine the ACF of microalgal cells: 1) a property measurement approach and 2) a particle tracking approach. The first method involved experimentally measuring the size distribution, density and compressibility of the cells and calculating the ACF. The second method utilized particle tracking velocimetry and a COMSOL Multiphysics model to estimate the ACF. The ACF was characterized, using both techniques, for three species—*Chlamydomonas reinhardtii*, *Nannochloropsis salina*, and *Tetraselmis chuii*—as a function of dynamic cellular composition over a 2-week growth period. For *C. reinhardtii* the lipid content increased from 26% ± 1% to 40% ± 1% from day 3 to 9, which resulted in a 43% decrease in ACF (0.056 ± 0.003 to 0.032 ±

0.001). For *N. salina* the lipid content increased from 25% ± 1% to 33% ± 1% from day 3 to 10, which also resulted in a 43% decrease in ACF (0.040 ± 0.002 to 0.023 ± 0.001). For *T. chuii* the lipid content remained relatively stable (~10%) throughout the growth period so the ACF (~0.3) did not change significantly. ACF decreases as lipid content increases because lipids have a negative ACF in growth media, whereas carbohydrates and proteins have a positive ACF. However, cell size can have a greater impact on an algal strains' responsiveness to acoustic harvesting because the net force is proportional to Φa^2. Furthermore, acoustic harvesting works best for large diameter cells, provided that those cells have a nonzero ACF. *T. chuii* had the largest cell diameter of approximately 12 µm, while *C. reinhardtii* and *N. salina* had cell diameters of 8.5 µm and 4.3 µm, respectively. The Φa^2 values for *T. chuii* were approximately 50× higher than the values for *N. salina,* which is largely due to *T. chuii* cells having a diameter that is 3× the diameter of *N. salina* cells. Composition also contributed to the higher Φa^2 values for T. chuii since these cells were composed of mostly carbohydrates and had an ACF that was an order of magnitude higher than the ACF of *N. salina*. This research shows that acoustic harvesting has the potential to positively impact the algal biofuels value chain through the reduction of energy required for harvesting.

ACKNOWLEDGEMENTS

I would like to express my sincere gratitude for the guidance and support of my three advisors: Dr. Anthony Marchese, Dr. Jason Quinn, and Dr. Jessica Tryner. Thank you for your expert knowledge, mentorship, advice, and patience through this process. I would also like to thank the two undergraduate research assistants that helped me with experiments in the lab: Kara Gustafson and Micah Bush. Thank you to Derek Hess, Allison Werner, Mirna Ayshoa, Peter Chen, Jacob Sebesta, and Carlos Quiroz for providing laboratory guidance and answering any questions I had about algae. Thank you to Dr. Hincapié Gómez for answering questions about previous work on acoustic harvesting. Thank you to Barbara Bernstein for taking the confocal microscope images of the algae. Thank you to the Department of Energy grant DE-EE0007089. Last but not least, I would like to thank my friends and family for being loving and supportive.

TABLE OF CONTENTS

ABSTRACT ii
ACKNOWLEDGEMENTS iv
1 INTRODUCTION 1
1.1 Motivation 1
1.2 Acoustophoresis 3
1.3 Previous Research on Acoustic Properties of Algae 6
2 MATERIALS AND METHODS 8
2.1 Microalgae Cultures and Cultivation 8
2.1.1 Algal Concentration Quantification 10
2.2 Determination of Algal Composition 10
2.2.1 Lipid Quantification 11
2.2.2 Protein Quantification 11
2.2.3 Carbohydrate Quantification 12
2.2.4 Ash Quantification 12
2.3 Determination of the Acoustic Contrast Factor 13
2.3.1 Property Measurement Approach 13
2.3.2 Particle Tracking Approach 16
3 RESULTS AND DISCUSSION 21
3.1 Impact of Cellular Composition on Acoustic Contrast Factor 22
3.1.1 Variation in Cellular Composition Over the Growth Cycle 22
3.1.2 Acoustic Contrast Factor Determined by the Property Measurement Approach 24
3.1.3 Acoustic Contrast Factor Determined by the Particle Tracking Approach 29
3.2 Impact of Cell Size on Harvesting Performance 31
4 CONCLUSION 35
REFERENCES 37
APPENDIX I 43

LIST OF TABLES

Table 1. Density, speed of sound, compressibility, and acoustic contrast factor in saline growth media for various substances. [25]..... 5

Table 2. Amount of algae used in experiments and corresponding cell concentrations..... 14

Table 3. Cellular composition on each acoustic measurement day for *C. reinhardtii*, *N. salina*, and *T. chuii*. Central values represent the average and the numbers in parentheses represent the total range in measurements..... 22

Table 4. Variations in Cell size (average diameter, average cell volume, and diameter of average volume), cell properties (density and compressibility), and ACF of the cells in their respective growth media (property measurement approach and particle tracking approach) over the growth cycle for three microalgae strains. The uncertainty in the cell diameter is the standard deviation. For cell volume and diameter of average volume, the uncertainty is the 95% confidence interval on the mean. For cell density and compressibility the uncertainty is the standard deviation between each dilution sample. The uncertainty in the ACF represents the propagation of error due to the uncertainty in either average cell volume (for the property measurement approach) or cell diameter (for the particle tracking approach)..... 26

LIST OF FIGURES

Figure 1. Demonstration of algal cells undergoing the acoustic radiation force under a microscope (left) and in a 4 mL quartz cuvette (right). The blue line represents the ultrasonic standing wave and the cells are agglomerating at the nodes of this wave. 4

Figure 2. Photobioreactor system used to grow algae in this study. PBRs were kept in a thermal bath to maintain culture temperature and pH was controlled with CO_2 air sparging. 9

Figure 3. PTV experimental setup. The cuvette with algae or polyamide particle sample was placed under the microscope that was coupled to a camera (left). The driving piezoelectric disc was epoxied to one side of the cuvette and the sensing piezoelectric disc was attached to the opposite side with ultrasound gel for each experiment (right). 18

Figure 4. Process diagram of how the experimental setup was assembled. The base of each arrow indicates the output while the tip of each arrow indicates the input. 18

Figure 5. Growth curves for *C. reinhardtii*, *N. salina*, and *T. chuii*. Markers represent the average concentration of the 9-12 individual PBR tubes and the error bars represent the standard deviation. The acoustic properties and composition were measured on days 3, 6, and 9 for *C. reinhardtii*; days 3, 7, and 10 for *N. salina*; and days 3, 6, 9, and 14 for *T. chuii*. Filled markers represent the acoustic measurement days. 21

Figure 6. Density (left) and compressibility (right) of suspensions of *C. reinhardtii*, *N. salina*, and *T. chuii* in growth media as a function of the volume fraction of cells in the media on each acoustic measurement day. 25

Figure 7. Cell composition as a function of acoustic measurement day is represented by the bar graphs and the left axis. ACF on each day, as determined by property measurement approach (green) and particle tracking approach (orange), is shown by the points and right axis. Error bars represent the propagation of the uncertainty in cell size. For *T. chuii*, the ACF for Day 9 was not calculated with the particle tracking approach. 28

Figure 8. Motion of three randomly chosen *C. reinhardtii* (left), *N. salina* (middle), and *T. chuii* (right) cells on each acoustic measurement day measured using PTV in the solid lines. Shaded areas represent COMSOL modeling of where each cell should be with the range due to the standard deviation of the cell size on each day and the corresponding ACF. 30

Figure 9. Histogram of cell size for *C. reinhardtii* (left), *N. salina* (middle), and *T. chuii* (right) on each acoustic measurement day. The average diameter for *C. reinhardtii* was 8.5 µm, 8.0 µm, and 8.5 µm on day 3, 6, and 9, respectively. For *N. salina*, the average diameter on each day was 4.3 µm. For *T. chuii*, the average effective diameter was 12.5 µm, 11.0 µm, and 13.0 µm, and 11.5 µm on Day 3, 6, 9, and 14, respectively. The histogram for day 14 can be found in Appendix I. 33

Figure 10. Acoustic contrast factor (property measurement approach) multiplied by the effective cell radius squared ($a^2\Phi$) over the growth cycle for each algal strain. This metric is proportional to the ratio of the acoustic radiation force to the drag force. Blue bars represent *N. salina*, green bars represent *C. reinhardtii*, and orange bars represent *T. chuii*. The y-axis is on a log 10 scale. 34

Figure 11. Histogram of cell size *T. chuii* on Day 14. The average effective diameter is 11.5 µm. 43

1 INTRODUCTION

1.1 **Motivation**

Climate change is an urgent, global issue that must be combated to reduce the risks of sea level rise, temperature changes, and more intense storms [1] [2]. Reducing CO_2 emissions from the use of liquid transportation fuels could reduce the effects of climate change. Biofuels made from microalgae have the potential to make transportation more sustainable by decreasing lifecycle greenhouse gas emissions [3] reducing the dependence on imported fuels [4]. Biofuels made from microalgae have the ability to reduce greenhouse gas emissions by 50% or more compared to fuels made from petroleum, allowing for the possibility for algae biofuels to qualify as advanced biofuels under the Renewable Fuel Standard [5] [6] [7]. Microalgae are one of the only biofuel sources that have the productivity required for global-scale production [8]. Microalgae have a production rate that is 10 to 100 times higher than that of terrestrial biofuel crops [9]. Additionally, microalgae have an advantage over more traditional biofuel crops, such as corn and switchgrass, because they do not require land that would otherwise be used for agriculture [10]. Microalgae grow in water and some strains can even thrive in salt water or wastewater [8] [11]. Microalgae also consume carbon dioxide at a rate of 1.83 kg of carbon dioxide per kilogram of biomass [12]. Therefore, microalgae farms co-located with power plants could recycle CO_2 and temporarily reduce the amount released into the atmosphere [12] [13]. Another benefit of microalgae is that it can be used as animal feed because it has a similar profile to the Food and Agricultural Organization reference case for conventional foods and can store up to 54% dry weight as protein [14]. Microalgae are also becoming more widespread in the cosmeceuticals, nutraceuticals, and functional foods industries due to their high-value products

such as β-carotene, astaxanthin, docosahexaenoic acid, eicosahexaenoic acid, and phycobilin pigments [15].

Currently, a major setback with producing microalgae as a biofuel feedstock or bioproduct is the dewatering process due its' high energy input and cost. Many lifecycle and techno-economic analyses show that microalgal biofuels are not economically or energetically viable yet—partially due to this dewatering energy sink [16]. Microalgae cells are usually cultivated in large amounts of water and it is difficult to remove the cells because they have a similar density to water. The current practice for removing the microalgae is to use expensive, energy-intensive centrifuges or filter presses [17] [18]. An alternative approach to these energy intensive processes is using ultrasonic standing waves to harvest the cells.

Ultrasonically enhanced settling (UES), which is a form of acoustic harvesting, is a method used to separate particles in suspension with a liquid. Ultrasonic standing waves are applied to a liquid medium and cause particles in the solution to move together to form bands at the node or antinode of the wave. The particle movement as a result of the sound pressure is known as acoustophoresis. This technique has mostly been used for relatively small batch volumes and low throughput. UES has been used to separate red blood cells [19], hybridoma cells, Chinese hamster ovary cells [20], oil and water emulsions [21], milk, and palm oil [22]. A recent review of ultrasonic separation [22] only found one application for microalgae [23]. Ultrasonically enhanced settling has the potential to reduce the cost of algal biofuels associated with harvesting by about two orders of magnitude [24]. Depending on the responsiveness of algae to acoustic harvesting, this technology could consume less energy than centrifugation or membrane filtration, making it the only technology capable of meeting the National Alliance for Advanced

Biofuels and Bioproducts goal of bringing harvesting costs down to $0.013 per gallon of gasoline equivalent [24] [25].

1.2 **Acoustophoresis**

The phenomenon of particle migration due to acoustic waves is known as acoustophoresis. Acoustic waves can be mathematically described by the wave equation in terms of the acoustic pressure [26]:

$$\frac{\partial^2 p}{\partial x^2} = \frac{1}{c^2}\frac{\partial^2 p}{\partial t^2} \quad (1)$$

where p is the acoustic pressure (Pa), x is the distance coordinate (m), c is the speed of sound ($m \cdot s^{-1}$) and t is the time (s). A standing wave is a special case in which an acoustic wave ends on a rigid boundary condition, such as a reflecting surface. The wave is fully reflected with a 180° phase difference, creating a constructive interference. The resulting standing wave has twice the amplitude of the original acoustic wave (due to the constructive interference) with minimal power leaving the fluid [27].

Ultrasonic standing waves have been used to manipulate particles in a fluid [28]. A spherical particle in suspension with a fluid becomes a scattering point, or compressibility mismatch, for the acoustic wave, which creates the acoustic force on the sphere [29]. The acoustic radiation force pushes the particles to the acoustic nodes or antinodes and is dependent on the acoustic contrast factor (ACF) and the radius of the particle cubed [30]:

$$F_{rad} = 4\pi\Phi k a^3 E_{ac} \sin(2kz) \quad (2)$$

where k is the wavenumber (m^{-1}), a is the radius of the particle (m), E_{ac} is the acoustic energy density ($J \cdot m^{-3}$), z is the position of the particle along the axis of the standing wave (m), and Φ is the acoustic contrast factor [31]:

$$\Phi = \frac{1}{3}\left[\frac{5(\rho_p/\rho_m) - 2}{2(\rho_p/\rho_m) + 1} - \frac{\kappa_p}{\kappa_m}\right] \quad (3)$$

where ρ_p is the density (kg·m^{-3}) of the particle (an algal cell in this case), ρ_m is the density (kg·m^{-3}) of the fluid (growth media in this case), and κ_p and κ_m are the compressibility of the particle and fluid, respectively, (Pa^{-1}). Compressibility is related to density and speed of sound as shown in Equation 4:

$$\kappa = \frac{1}{\rho c^2} \quad (4)$$

where c is the speed of sound (m·s^{-1}).

The theory behind Equations 2 and 3 is based on the case when the particle radius is small compared to the sound wavelength and when the particle and liquid densities are the same order of magnitude. The acoustic radiation force causes the cells to migrate to the node of the ultrasonic standing wave when the ACF is positive, as seen in Figure 1. When the ACF is negative, the cells will instead migrate to the antinode of the wave [30] [32].

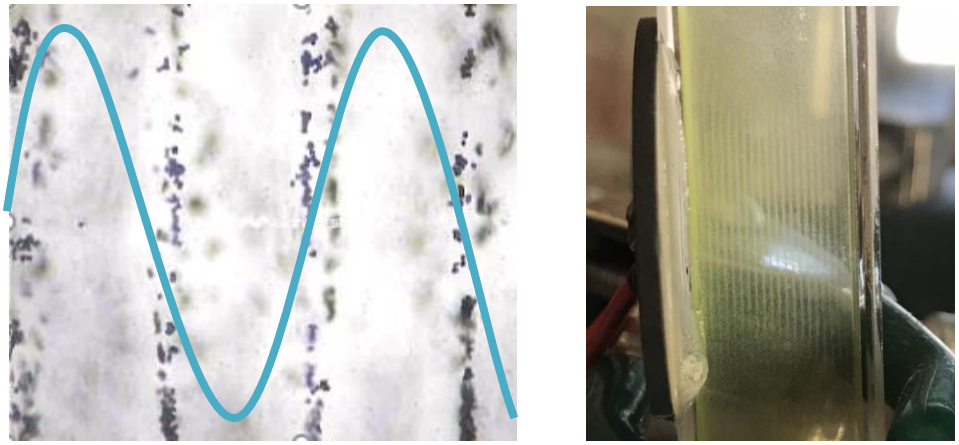

Figure 1. Demonstration of algal cells undergoing the acoustic radiation force under a microscope (left) and in a 4 mL quartz cuvette (right). The blue line represents the ultrasonic standing wave and the cells are agglomerating at the nodes of this wave.

Cell composition determines whether the ACF of algal cells will be positive or negative.

Microalgae cells are primarily composed of lipids, proteins, and carbohydrates. Particles composed of pure protein or pure carbohydrate would have a positive ACF when suspended in algal growth media, while particles composed of pure lipid would have a negative ACF (Table 1). Cells with high lipid content are desired for algal biofuel production. As algal cells accumulate lipids over their growth cycle, it is possible that the ACF of the cells in the media could approach zero or become negative [25]. For acoustic harvesting to work, the ACF needs to be positive or negative, but not zero. This research investigates changes in cell composition to determine if acoustic harvesting would become ineffective over the course of a growth period.

Table 1. Density, speed of sound, compressibility, and acoustic contrast factor in saline growth media for various substances. [25]

Substance	Density, ρ ($kg \cdot m^{-3}$)	Speed of sound, c ($m \cdot s^{-1}$)	Compressibility, κ (Pa^{-1})	Acoustic contrast factor in media, Φ (-)
Water @ 20 °C [25]	998	1483	4.56×10^{-10}	-
Saline growth media [25]	1013	1504	4.37×10^{-10}	-
Carbohydrates (corn starch) [33]	1620	2810	7.82×10^{-11}	0.42
Protein (Myoglobin) [34]	1370	3473	6.05×10^{-11}	0.38
Lipid @ 20 °C (soybean oil) [25]	919	1470	5.03×10^{-10}	-0.08
Microalgae (*Chlorella vulgaris*) [35]	1100	1540	3.83×10^{-10}	0.07
Polyamide seeding particles [36]	1030	2200	2.01×10^{-10}	0.19

Cell size is another parameter that impacts the responsiveness to acoustic harvesting. The acoustic radiation force is proportional to the cell radius cubed (Equation 2). However, when algal cells are suspended in media the acoustic radiation force is opposed by a drag force from movement in a viscous fluid:

$$F_D = C_D A \frac{\rho_m V^2}{2} \tag{5}$$

where C_D is the drag coefficient, A is the cross-sectional area of the cell (m^2), and V is the velocity of the cell ($m \cdot s^{-1}$).

Assuming a spherical cell, the coefficient of drag is given by Equation 6 when $Re \lesssim 1$, and the resulting drag force is given by Equation 7:

$$C_D = \frac{24}{Re} = \frac{24\mu_m}{D\rho_m V} \tag{6}$$

$$F_D = 6\pi\mu_m V a \tag{7}$$

where μ_m is the dynamic viscosity of the media ($kg \cdot m^{-1}s^{-1}$). Therefore, the ratio of the acoustic radiation force to the drag force is proportional to Φa^2. This metric was chosen to compare algal cells in specific growth conditions to determine which cells would be more readily harvested.

1.3 **Previous Research on Acoustic Properties of Algae**

Prior to this work, limited data were available on the manner in which the acoustic response of microalgae cells varies with strain, growth conditions, and growth stage. Hincapié Gómez et al. (2018) calculated ACFs for *M. gaditana, N. oculata, P. tricornutum,* and *C. reinhardtii* by measuring the density and speed of sound of the cells in suspension (see Section 2.3.1) [25]. This approach involved measuring the density and sound velocity of algal cells suspended in media and then calculating a restulting density and sound velocity of the algal cells. The ACF of *C. reinhardtii* was also measured by using particle tracking velocimetry to record the motion of the cells in the presence of an acoustic field (see Section 2.3.2). The recordings of cell motion were matched with COMSOL Multiphysics modeling to infer an ACF based on other known quantities in Equation 2 [25].

The ACF of microalgae cells (in fresh water or salt water growth media) could theoretically be positive or negative depending on cellular composition since the ACFs of carbohydrates and

proteins are positive and the ACF of lipids is negative. Therefore, the ACF of microalgae cells could change dramatically as cells grow and accumulate lipids. Hincapié Gómez et al. (2018) demonstrated this concept experimentally using starch null sta6 mutant *C. reinhardtii* (CC-4348) cells [25]. The cells were cultured in a nutrient-rich medium and were then transferred to a nitrogen-depleted medium and boosted with acetate. Cells cultivated using this procedure have been shown to accumulate large lipid bodies and eventually become less dense than water [37] [38]. The impact of cellular composition on ACF was explored by performing PTV measurements on cells harvested at the beginning, intermediate, and end stages of the nine-day post-boost, nitrogen-deprived growth period [25]. At the beginning of the growth period, the cells had a positive ACF and migrated to the node of the standing wave. Mid-way through the growth period, the cells did not respond to the acoustic field, indicating that the ACF was very close to zero. At the end of the growth period, the cells had a negative ACF and migrated to the antinode of the standing wave [25]. These results demonstrate that changes in cellular composition over the course of the growth cycle can impact both the magnitude and the sign of the ACF.

Although Hincapié Gómez et al. (2018) demonstrated that acoustic properties can vary depending on algal strain and growth stage, they did not quantitatively measure cell carbohydrate, protein, and lipid contents at any point in the growth process [25]. Furthermore, the previous study did not report quantitative variations in ACF over the course of the growth cycle. In the present study, the acoustic contrast factor and cell composition (e.g., lipid, protein, and carbohydrate content) were evaluated for three microalgae strains at the beginning, middle, and end of 9 to 14 day growth periods to quantitatively determine impact of the variation in cell composition on acoustic properties. The discussion section focuses on the impact of a dynamic ACF on the implementation of acoustic harvesting systems.

2 MATERIALS AND METHODS

The acoustic contrast factors for three species of microalgae (*Chlamydomonas reinhardtii, Nannochloropsis salina,* and *Tetraselmis chuii*) were determined by measuring the density and speed of sound of suspensions of microalgae cells in growth media. In addition, the trajectories of microalgae cells exposed to an acoustic field were measured using particle tracking velocimetry (PTV) and modeled using COMSOL Multiphysics to determine the effective ACF of the cells in the media. Both of these methods were used to study how ACF changes as microalgae accumulate lipids and change composition throughout a batch growth cycle.

2.1 **Microalgae Cultures and Cultivation**

Chlamydomonas reinhardtii isoamaylase deficient mutant (CC-4334) was obtained from the Chlamydomonas Resource Center. As described in Hincapié Gómez et al. (2018), the strain was cultivated phototrophically in tris-acetate-phosphate (TAP) in a 9 L photobioreactor (PBR) (Figure 2) at 23 °C and 350 $\mu mol \cdot m^{-2} \cdot s^{-1}$ of continuous light [25]. A mixture of air and carbon dioxide was bubbled through the system to maintain a pH of 7 [25]. The density, speed of sound, cell size, motion of the cells in the presence of an acoustic standing wave, and cell composition were measured after 3, 6, and 9 days of growth.

Nannochloropsis salina (CCMP 1776, recently reclassified as *Microchloropsis salina*) was obtained from the Bigelow National Center for Marine Algae and Microbiota. The microalgae were cultivated phototrophically with autoclaved *N. salina* growth medium (described by Napan et al. [39]) in a 12 L photobioreactor (Figure 2) at 23 °C and 350 $\mu mol \cdot m^{-2} \cdot s^{-1}$ of continuous light. A mixture of air and carbon dioxide was bubbled through the system to maintain a pH of 7. The

density, speed of sound, cell size, motion of the cells in the presence of an acoustic standing wave, and cell composition were measured after 3, 7, and 10 days of growth.

Tetraselmis chuii (UTEX LB 232) was obtained from the Culture Collection of Algae at The University of Texas at Austin (UTEX). The microalgae were cultivated phototrophically in f/2 media in a 12 L photobioreactor (Figure 2) at 24 °C and 350 $\mu mol \cdot m^{-2} \cdot s^{-1}$ of continuous light. A mixture of air and carbon dioxide was bubbled through the system to maintain a pH of 7.5. The density, speed of sound, cell size, motion of the cells in the presence of an acoustic standing wave, and cell composition were measured after 3, 6, 9, and 14 days of growth.

Each of the three microalgae strains (*C. reinhardtii, N. salina,* and *T. chuii*) were cultivated in nine to twelve separate PBRs, depending on the strain. On each sample day, equal volumes from each tube were taken and mixed together to form a stock solution so that enough biomass would be available for all of the subsequent analyses, which included cell size imaging, density meter testing, PTV, and composition analyses.

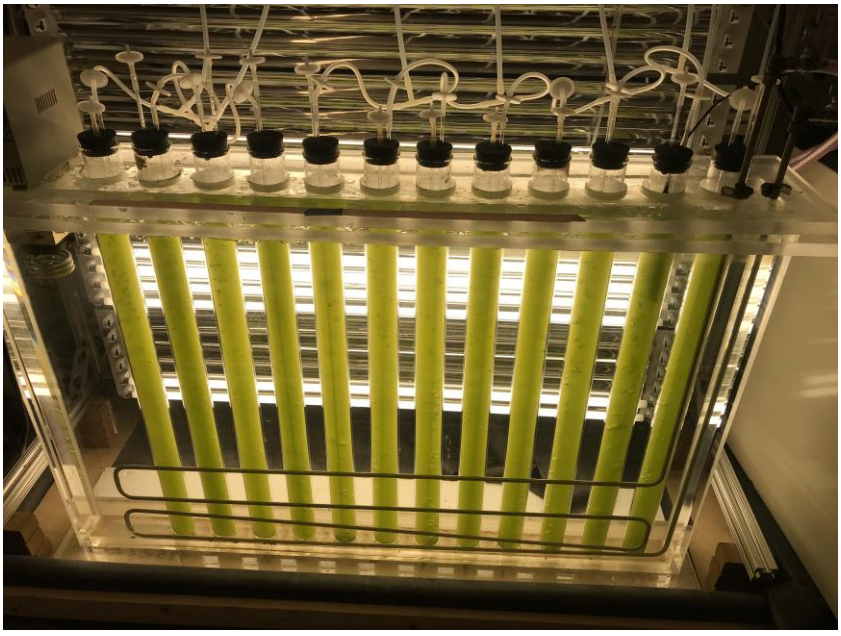

Figure 2. Photobioreactor system used to grow algae in this study. PBRs were kept in a thermal bath to maintain culture temperature and pH was controlled with CO_2 air sparging.

2.1.1 Algal Concentration Quantification

Periodic measurements of algal concentration were taken to track algal growth. The vacuum filtration method was used to create a correlation curve between algal concentration and optical density measured at 750 nm [40]. Multiple aliquots of algal suspensions at optical densities ranging from 0.1 – 0.9 were filtered through glass fiber filters (Whatman GF/F, 47 mm, nominal pore size 0.7 μm). Each optical density sample had five replicates of 5 mL each. The control used 5 mL of media instead of an algal suspension. Each pre-weighed filter was rinsed with 1 mL of deionized (DI) water before adding the 5 mL sample. After the sample was added, the vacuum was turned on for at least 10 minutes. Filter papers were dried in a 40°C oven for 48 hours. After drying, filters were re-weighed to the nearest 0.0001 g. Water absorbed to the filter from the relative humidity in the air was assumed to be negligible as filters were weighted within 2 minutes of being removed from the oven. The difference in filter weight was used to determine the mass concentration of algae at each optical density reading [40]. During the algal growth cycles, the optical density was measured and the calibration curve was utilized to estimate the concentration of algae.

2.2 **Determination of Algal Composition**

The ACF and cell composition were evaluated at different points in the algal growth cycle to determine how changing cell composition affected acoustic properties. *C. reinhardtii* was evaluated on day 3, 6, and 9 of the growth cycle; *N. salina* was sampled on day 3, 7, and 10; and *T. chuii* was sampled on day 3, 6, 9, and 14. The methods used to quantify cell composition (i.e., lipid, protein, carbohydrate, and ash content) are described below. In preparation for the composition measurements, the algae stocks were freeze dried in a lyophilizer (FreeZone 2.5, Labconco, Kansas City, MO, USA) at -50°C and 0.020 mBar for 48 hours. The Tukey-Kramer

multiple comparisons procedure was used with $\alpha = 0.05$ to determine if the composition of a strain changed significantly between sample days [41].

2.2.1 Lipid Quantification

A sulfo-phospho-vanillin (SPV) colorimetric method described by Mishra et al. (2014) was used to determine the lipid content of each algal strain on separate days in the growth cycle [42]. Canola oil (120962-03-0, Sigma Aldrich, St. Lois, MO, USA) was used as the lipid standard to create the calibration curve [42]. To make the algal stock solutions, approximately 10 mg of freeze-dried algae were crushed with a mortar and pestle and mixed with 10 mL of DI water in a test tube. The only modification made to the procedure of Mishra et al. (2014) was that each test tube was vortexed for 10 seconds after the addition of phospho-vanillin solution [42]. This modification allowed for better mixing in the incubator shaker. All samples were analyzed in triplicate at 530 nm using a spectrophotometer (Genesys 20, Thermo Scientific, Waltham, MA, USA).

2.2.2 Protein Quantification

The Modified Lowry Protein Assay kit (P123240, Thermo Scientific, Waltham, MA, USA) was utilized to quantify the algal protein content [43]. To make the algal stock solutions, 10 mg of freeze-dried algae were ground in a mortar and pestle and suspended in 5 mL of lysis buffer to facilitate the extraction of proteins [44]. To prevent any interference caused by the lysis buffer, the stock solution was vortexed with a sodium dodecyl sulfate salt (SDS) solution as described in González López et al. (2010) [44]. Albumin (BSA) dissolved in lysis buffer was used as the standard to create the calibration curve [44]. All samples were centrifuged at 3000 g for 3 minutes to remove any particles [45]. All samples were analyzed in triplicate at 750 nm using a spectrophotometer (Genesys 20, Thermo Scientific, Waltham, MA, USA).

2.2.3 Carbohydrate Quantification

The Sulfuric Acid – UV method was used to quantify the carbohydrate content in each algal strain [46]. This procedure is a newer, faster alternative method to the Phenol-Sulfuric Acid method [47], the latter of which is more hazardous due to the use of phenol [46]. The Sulfuric Acid – UV method also cuts measurement error in half [46]. Two calibration curves were created using glucose and starch as standards [48]. The average of these two curves was used to represent a calibration curve for neutral carbohydrates [46]. To make the algal stock solutions, approximately 10 mg of freeze-dried algae were crushed with a mortar and pestle and mixed with 10 mL of DI water. To obtain carbohydrate concentrations in the range of the calibration curve, the stock solution was diluted 10 fold with DI water. The only modification made to the Sulfuric Acid – UV procedure was that the test tubes were vortexed before and after the ice bath. All samples were analyzed in triplicate at 315 nm using a UV-VIS spectrophotometer (NanoDrop 2000, Thermo Scientific, Waltham, MA, USA).

2.2.4 Ash Quantification

Ash content for saltwater species (*N. salina* and *T. chuii*) were analyzed using the National Renewable Energy Laboratory's Analytical Procedure [49]. This method involved placing 100 mg samples, which were contained in aluminum weigh boats (08-732-101, Fisher Scientific, Hampton, NH, USA), inside a muffle furnace (Thermonace FB1315M, Thermo Scientific, Waltham, MA, USA). Samples were then heated in accordance with the following program [49]:

- Ramp from room temperature to 105 °C and hold for 12 minutes
- Ramp to 250 °C at 10 °C per minute and hold for 30 minutes
- Ramp to 575 °C at 20 °C per minute and hold for 180 minutes

- Allow temperature to drop to 105 °C and hold until samples are removed and placed into a desiccator to cool to room temperature

Samples were completed in triplicate and were weighed in an analytical balance (HPB414Ai, Veritas, Mountain View, CA, USA) to the nearest 0.1 mg. Ash content for freshwater species *C. reinhardtii* was assumed to be negligible [50].

2.3 **Determination of the Acoustic Contrast Factor**

The methods used to measure ACF were previously described by Hincapié Gómez et al. (2018), but a summary is included here [25]. Two different methods were used to determine the ACF: 1) property measurement approach and 2) particle tracking approach. The property measurement approach involved calculating the density and sound velocity of microalgae cells and subsequently using these values to directly calculate the ACF. The particle tracking approach involved recording videos of the microalgae cell motion under the acoustic force and utilized particle tracking velocimetry and COMSOL modeling to determine the ACF. The Tukey-Kramer multiple comparisons procedure was used with $\alpha = 0.05$ to determine if the ACF of a strain changed significantly between sample days [41].

2.3.1 Property Measurement Approach

A stock solution of each algal strain was created by mixing an equal volume from each 1 L tube in the photobioreactor to total the final volume given in Table 2. About 10 mL was set aside for both cell size imaging and PTV testing. Part of the algae quantity taken from the PBR was set aside for composition testing (Table 2), and the rest was retained for density and speed of sound measurements. The stock algae solutions to be used for density/speed of sound measurements and composition tests were centrifuged to separate the cells from the media. *C. reinhardtii* samples were centrifuged at 2990 g for 5 minutes. *N. salina* samples were centrifuged at 2850 g for 20

minutes. *T. chuii* samples were centrifuged at 1050 g for 10 minutes. The centrifuged cells to be used for composition testing were placed in a -80 degree freezer. The centrifuged cells to be used for density and speed of sound measurements were re-suspended in the media used to grow those cells to obtain a concentrated mixture with a volume of approximately 5 to 13 mL. This concentrated mixture was then diluted with media to create five suspensions with a range of cell concentrations shown in Table 2, which were used to measure acoustic properties.

Table 2. Amount of algae used in experiments and corresponding cell concentration ranges for the concentrated suspensions used for the density and speed of sound measurements.

Strain	**Sample day**	**Algae sample taken from PBR (mL)**	**Algae sample for composition tests (mL)**	**Cell concentration (cells·mL^{-1})**
C. reinhardtii	3	540	315	$8.7 \times 10^7 – 1.7 \times 10^9$
	6	540	315	$5.6 \times 10^7 – 1.3 \times 10^9$
	9	540	315	$7.3 \times 10^7 – 1.7 \times 10^9$
N. salina	3	600	240	$1.6 \times 10^9 – 9.1 \times 10^9$
	7	600	240	$2.6 \times 10^9 – 1.3 \times 10^{10}$
	10	600	240	$3.2 \times 10^9 – 1.5 \times 10^{10}$
T. chuii	3	960	480	$9.5 \times 10^6 – 5.6 \times 10^7$
	6	960	480	$1.8 \times 10^7 – 1.5 \times 10^8$
	9	960	480	$2.3 \times 10^7 – 1.5 \times 10^8$
	14	960	480	$2.5 \times 10^7 – 1.6 \times 10^8$

For each strain, a correlation curve for cell concentration (# cells·L^{-1}) and optical density was created by using a hemocytometer. On each side of the hemocytometer, five grid sections were used to count cells (top right, bottom right, top left, bottom left, and center) [51]. Optical density and cell count were measured for three dilutions of each algal strain to confirm the linear trend between these two quantities. On each acoustic measurement day, optical density was measured on each of the five aliquots used in the density meter testing. Cell concentration was calculated using the previously determined linear trend between optical density and cell count. The

volume fraction of microalgae in each aliquot was determined by multiplying the cell concentration by the average cell biovolume for the given strain.

For *C. reinhardtii* (CC-4334) and *T. chuii* (UTEX LB 232), cell size was measured using an Olympus IX81 inverted spinning disk confocal (SDC) microscope with a 20X objective lens coupled to a Photometrics Cascade II EMCCD camera. For *N. salina* (CCMP 1776), the same setup was used except a 40X objective lens was coupled to the camera because these cells were much smaller. A micron slide was used to determine the number of pixels per micrometer in each photograph. The diameters of 200-400 cells were determined by analyzing images manually using Image J (https://imagej.net). Average biovolume was evaluated assuming that *C. reinhardtii* and *N. salina* cells were spherical. The assumed shape for *T. chuii* cells was prolate spheroid [52]. The height and width of each *T. chuii* cell was measured and a volume was calculated assuming a prolate spheroid shape. Then, the effective diameter of a sphere of equal volume was calculated. This effective diameter is reported because the theory presented is based on spherical particles [29]. The average effective diameter was used to determine the ACF in the particle tracking approach described in Section 2.3.2. For the property measurement approach, the average volume (calculated using the measured height and width) was used to determine the volume fraction. On each acoustic measurement day, the average cell volume determined from the Image J measurements was used to calculate the volume fraction of cells in the media.

Density and sound velocity for each aliquot of varying cell volume fraction were measured using a DSA 5000 M Density and Sound Velocity Meter (Anton-Parr, Graz, Austria). The DSA 5000 M uses an oscillating U-tube to measure density and an ultrasonic transmitter and receiver to measure sound velocity. Each algal suspension, and pure media, were measured at 20 °C. On each acoustic measurement day, the calibration of the instrument was checked using room air and

deionized water. Before and after each sample set, the DSA 5000 M was rinsed with naphtha, acetone, and ethanol to clean the instrument. Media was used to rinse the sample chamber in between each sample. Approximately 3 mL of each algal sample was run through the instrument to record measurements.

For each sample, the density, compressibility, and speed of sound of the cells were calculated using Equations 8, 9, and 4, respectively [53]:

$$\rho = v_p \rho_p + (1 - v_p)\rho_m \tag{8}$$

$$\kappa = v_p \kappa_p + (1 - v_p)\kappa_m \tag{9}$$

where ρ and κ are the density ($g \cdot cm^{-3}$) and compressibility (Pa^{-1}), respectively, of the suspension, v_p is the volume fraction of cells in the suspension, ρ_p and κ_p are the density and compressibility, respectively, of the cells, and ρ_m and κ_m are the density and compressibility, respectively, of the media.

On each acoustic measurement date, the density and speed of sound were measured for 5 suspensions containing different concentrations of microalgae cells. The cell density and compressibility were reported as the average of these 5 samples ± one standard deviation. A 95% confidence interval was calculated for the average cell volume, and the lower and upper limits of this interval were used to estimate the uncertainty associated with the cell volume fraction when calculating ACF using the property measurement approach. The accuracy of the instrument is 0.007 $kg \cdot m^{-3}$.

2.3.2 Particle Tracking Approach

The particle tracking approach was also used to determine the ACF of algal cells on each sample day. First, the motion of 20 μm polyamide seeding particles (PSP-20, Dantec Dynamics, Skovlunde, Denmark) due to the acoustic force was recorded using PTV and modeled in COMSOL

Multiphysics. The density and compressibility of the particles were known from the manufacturer, therefore the ACF could be confidently calculated. Then the acoustic energy density (E_{ac}) could be determined because it was the only unknown in Equation 2. This procedure was completed with the polyamide particles suspended in each media type to determine the acoustic energy density for each media. The experiment and modeling were then repeated with algal cells to obtain an effective acoustic contrast factor for the cells. The acoustic energy density was assumed to remain constant between experiments utilizing the same media.

The PTV system consisted of a 4 mL quartz cuvette with a 25-mm-diameter ceramic disc piezoelectric transducer (SM111, Steiner & Martins, Inc., Doral, FL, USA) on one side to generate the acoustic field. A function generator (33120A, Agilent Technologies, Santa Clara, CA, USA) produced the ultrasonic wave that was amplified by a 3 Watt RF power amplifier (603L, E&I, Rochester, NY, USA). Another piezoelectric disc was placed on the opposite wall of the cuvette to act as a sensing transducer. This was connected to a spectrum analyzer (E4401B, Hewlett Packard, Palo Alto, CA, USA) to determine the maximum resonant peak to choose the operating frequency in each experiment. This setup is shown in Figure 3 and Figure 4. In each media, the maximum resonant peak corresponded to a slightly different frequency. The operating frequency was set to 1.64 MHz, 1.66 MHz, and 1.68 MHz for *C. reinhardtii*, *N. salina*, and *T. chuii*, respectively. The motion of polyamide particles and microalgae cells was recorded using a monochrome imaging camera (PL-B741U, Pixelink, Gloucester, Ontario, Canada) coupled to a Nikon TMS inverted microscope. Tracker 2.6 software (http://physlets.org/tracker) was utilized to measure the distance individual particles or cells traveled between each frame of the videos.

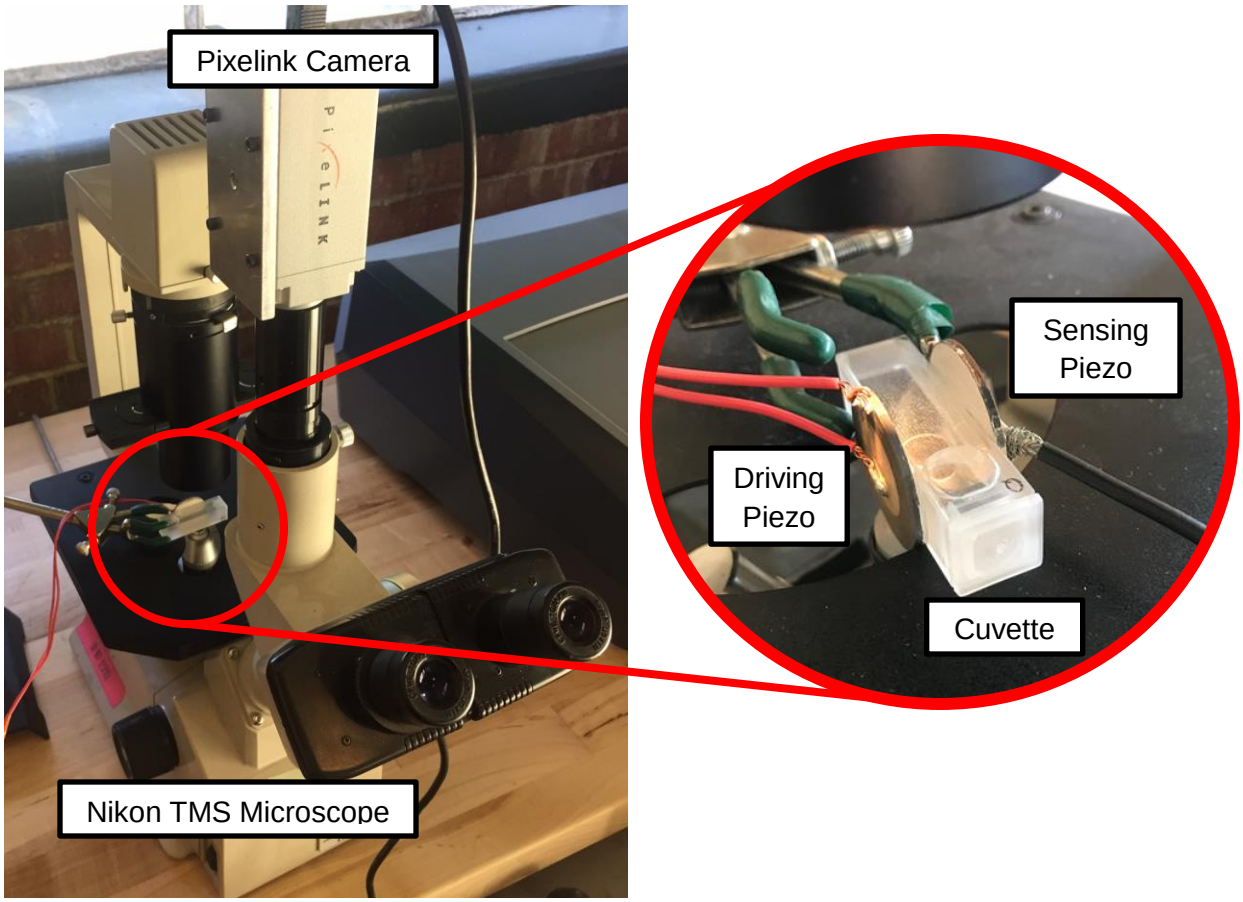

Figure 3. PTV experimental setup. The cuvette with algae or polyamide particle sample was placed under the microscope that was coupled to a camera (left). The driving piezoelectric disc was epoxied to one side of the cuvette and the sensing piezoelectric disc was attached to the opposite side with ultrasound gel for each experiment (right).

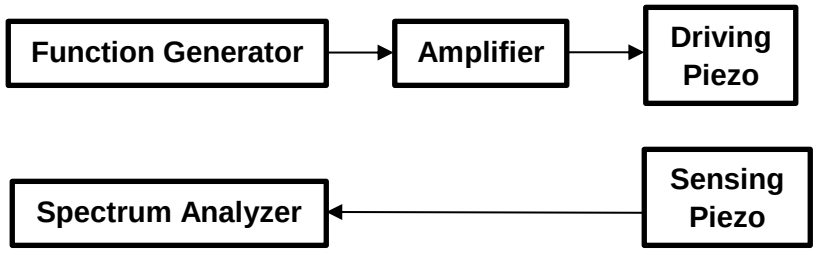

Figure 4. Process diagram of how the experimental setup was assembled. The base of each arrow indicates the output while the tip of each arrow indicates the input.

The Particle Tracing Module in COMSOL Multiphysics was used to create the model that predicted the motion of particles exposed to the acoustic field and the drag force. The acoustic radiation force was input as $F_{rad} = A \cdot \sin(2kz)$, where $A = 4\pi\Phi k a^3 E_{ac}$. The model was exercised for the polyamide particles with different values of E_{ac} until the velocity and acceleration profiles in the model agreed with the velocity and acceleration profiles measured experimentally using PTV. Agreement between the experiment and the model was obtained when the acoustic energy density was equal to 4.9 J·m^{-3} (using Φ = 0.196, k = 6936 m^{-1}, a = 10 μm) for the *C. reinhardtii* media. The acoustic energy densities for the *N. salina* media and *T. chuii* media were 6.5 J·m^{-3} (using Φ = 0.186, k = 6934 m^{-1}, a = 10 μm) and 0.8 J·m^{-3} (using Φ = 0.177, k = 6942 m^{-1}, a = 10 μm), respectively. Once the acoustic energy density was known, the only unknown for the microalgae cells was the ACF (Φ). To confirm the assumption that the acoustic energy density was constant in each media, the spectrum analyzer was used to ensure that the piezoelectric disc was operating at the maximum resonant frequency in each experiment.

The motion of three cells from different locations in a single culture was recorded on each sample date. The cell trajectories measured using Tracker were compared with the COMSOL Multiphysics model to determine the ACF using particle tracking approach. The cells were chosen at three different locations in respect to the node to ensure that the COMSOL model worked at any location. For each day, the model was manipulated to estimate the ACF to the nearest 0.01 of a cell with the average diameter. To assess the uncertainty associated with this ACF, the model was then adjusted to produce the trajectories of cells with the same ACF but with diameters equal to the average plus or minus the standard deviation of the cell diameter on that day. This created a shaded area in which the motion of a cell with the given ACF would be expected to fall. This shaded area was considered because cell size is a major factor in determining particle motion. If

the cell position trajectories of all three tracked cells fell within this shaded area, the ACF was confirmed. Uncertainty in the ACF was then quantified by adjusting the cell size in the model back to the average diameter and changing the ACF until the cell trajectory matched the trajectory of the larger or smaller cell (i.e. the edge of the shaded area).

3 RESULTS AND DISCUSSION

This section discusses the impact of cell size and cellular composition on the performance of ultrasonic harvesting of algae. This work improves upon previous research of Hincapié Gómez et al. (2018) by quantitatively assessing the impact of cellular composition on the acoustic contrast factor [25]. Acoustic properties were determined for three different strains of algae: *C. reinhardtii*, *N. salina*, and *T. chuii*. The acoustic contrast factor (ACF) for each strain was measured using two methods, 1) property measurement approach and 2) particle tracking approach, at a minimum of three temporally different points in the growth period. Growth curves for each strain are shown in Figure 5.

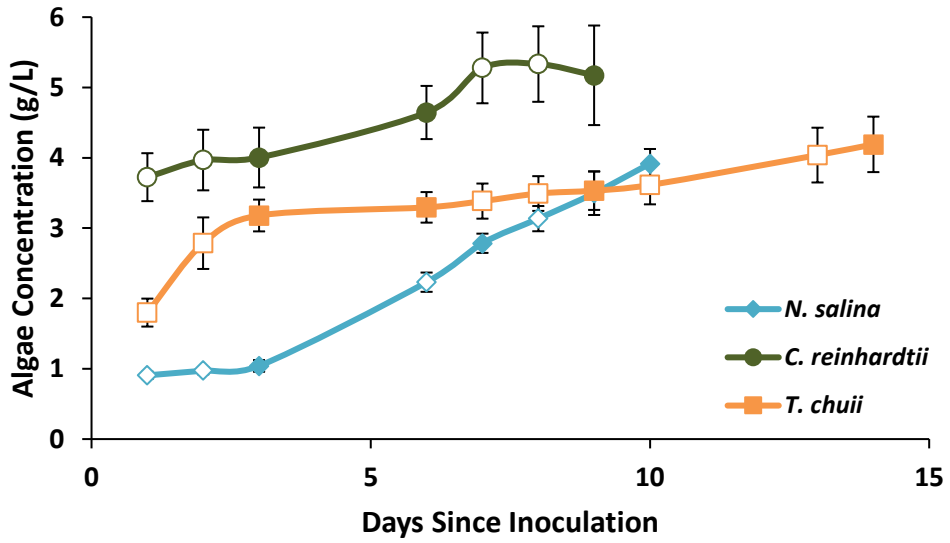

Figure 5. Growth curves for *C. reinhardtii*, *N. salina*, and *T. chuii*. Markers represent the average concentration of the 9-12 individual PBR tubes and the error bars represent the standard deviation. The acoustic properties and composition were measured on days 3, 6, and 9 for *C. reinhardtii*; days 3, 7, and 10 for *N. salina*; and days 3, 6, 9, and 14 for *T. chuii*. Filled markers represent the acoustic measurement days.

3.1 **Impact of Cellular Composition on Acoustic Contrast Factor**

3.1.1 Variation in Cellular Composition Over the Growth Cycle

The cellular composition of the algal cells varies over the course of the growth period. Cell composition on each acoustic measurement day for each algal strain is presented in Table 3. Percentages are presented in terms of ash free dry weight (AFDW) for saltwater species *N. salina* and *T. chuii*. *C. reinhardtii* was assumed to have a negligible ash content because it is a freshwater species [50]. The ash content for *N. salina* was 8.8% (7.8%, 10.3%), 6.0% (5.8%, 6.3%), and 5.2% (5.0%, 5.5%) on day 3, 7, and 10, respectively. The ash content for *T. chuii* was 13.7% (13.3%, 14.1%), 14.6% (13.8%, 16.3%), 19.6% (19.2%, 20.1%), and 20.5% (18.6%, 22.8%) on day 3, 6, 9, and 14, respectively. Since each composition experiment was completed in triplicate, central values above for ash content and in Table 3 represent the average and the numbers in parentheses represent the total range in replicates.

Table 3. Cellular composition on each acoustic measurement day for *C. reinhardtii, N. salina,* and *T. chuii*. Central values represent the average and the numbers in parentheses represent the total range in measurements.

Strain	Sample Day	Lipid %	Protein %	Carbohydrate %
C. reinhardtii	3	26 (25, 27)	38 (36, 39)	31 (25, 35)
	6	33 (32, 34)	35 (34, 36)	40 (39, 41)
	9	40 (39, 41)	26 (25, 27)	37 (34, 38)
N. salina	3	25 (24, 26)	22 (21, 23)	40 (37, 43)
	7	29 (28, 30)	15 (14, 16)	47 (44, 49)
	10	33 (32, 34)	15 (14, 16)	45 (44, 46)
T. chuii	3	9 (8, 10)	15 (14, 16)	94 (90, 101)
	6	10 (9, 11)	18 (17, 19)	88 (81, 97)
	9	12 (11, 13)	12 (11, 13)	91 (86, 95)
	14	12 (11, 13)	12 (11, 13)	80 (74, 83)

Algal cells are expected to accumulate lipids over the growth period as the culture becomes nutrient limited [54]. The lipid content increased substantially between each acoustic measurement day for *C. reinhardtii* and *N. salina*. For *C. reinhardtii*, the lipid content increased by 7 percentage points between each acoustic measurement day (from 26% ± 1% on day 3 to 40% ± 1% on day 9). For *N. salina*, the lipid content increased by 4 percentage points between each acoustic measurement day (from 25% ± 1% on day 3 to 33% ± 1% on day 10). For *T. chuii*, the lipid content remained relatively constant (at ~10%) throughout the 14-day growth period. In general the lipid increase in the cultures is expected based on nutrient limited growth [55] [56] [57].

The protein content of *C. reinhardtii* decreased by 3 percentage points from day 3 to 6 (38% ± 1% to 35% ± 1%) and decreased by 9 percentage points from day 6 to 9 (35% ± 1% to 26% ± 1%). The protein content of *N. salina* decreased by 7 percentage points between day 3 and day 7 (22% ± 1% to 15% ± 1%), but remained constant from day 7 to 10. The protein content of *T. chuii* remained relatively stable throughout the growth period. The carbohydrate content of all three strains did not change significantly from the beginning to the end of the growth period. For *T. chuii*, total values for AFDW composition are greater than 100%. This result is most likely due to uncertainty in the measurements because a large range in values for each measurement were obtained between replicates. The carbohydrate measurements, in particular, had a larger range compared to the other species. There are also cases for *C. reinhardtii* and *N. salina* where the total composition is less than 100%. This is due to the range in measurements and uncertainty associated with the procedures for measuring composition.

3.1.2 Acoustic Contrast Factor Determined by the Property Measurement Approach

Density and sound velocity measurements were taken on each acoustic measurement day for each algal strain using five dilutions of concentrated algae. Compressibility was calculated using Equation 4. As seen in Figure 6, density and compressibility varied linearly with volume fraction on each sample day (all R^2 values were greater than 0.97). Accordingly, Equations 8 and 9 were used to calculate the density and compressibility of the algal cells (Table 4). For *C. reinhardtii* and *N. salina*, density decreased and compressibility increased as the days since inoculation increased (see Figure 6). This result was expected because the fraction of lipids (which have a lower density than carbohydrates and proteins) in these cells increased as the growth cycle progressed. For *T. chuii*, density and compressibility remained relatively constant as the cellular composition did not change.

Since increases in lipid content caused the density of *C. reinhardtii* and *N. salina* cells to decrease and the compressibility to increase over the growth cycle, the ACF of the cells (calculated using Equation 3) decreased over time. The increase in lipid content drove the ACF down because lipids themselves have a negative ACF. The ACFs of *C. reinhardtii* and *N. salina* both decreased by 43% over the course of the growth cycle (Figure 7). Specifically, the ACF of *C. reinhardtii* decreased from 0.056 ± 0.003 to 0.032 ± 0.001 between days 3 and 9. The ACF of *N. salina* decreased from 0.040 ± 0.002 to 0.023 ± 0.001 between days 3 and 10. Conversely, the unchanging cellular composition for *T. chuii* yielded a relatively constant ACF of approximately 0.3, which is an order of magnitude higher than the ACF of the other species due to the low lipid content. These results demonstrate that accumulation of lipids over the growth period can make cells less responsive to the acoustic radiation force.

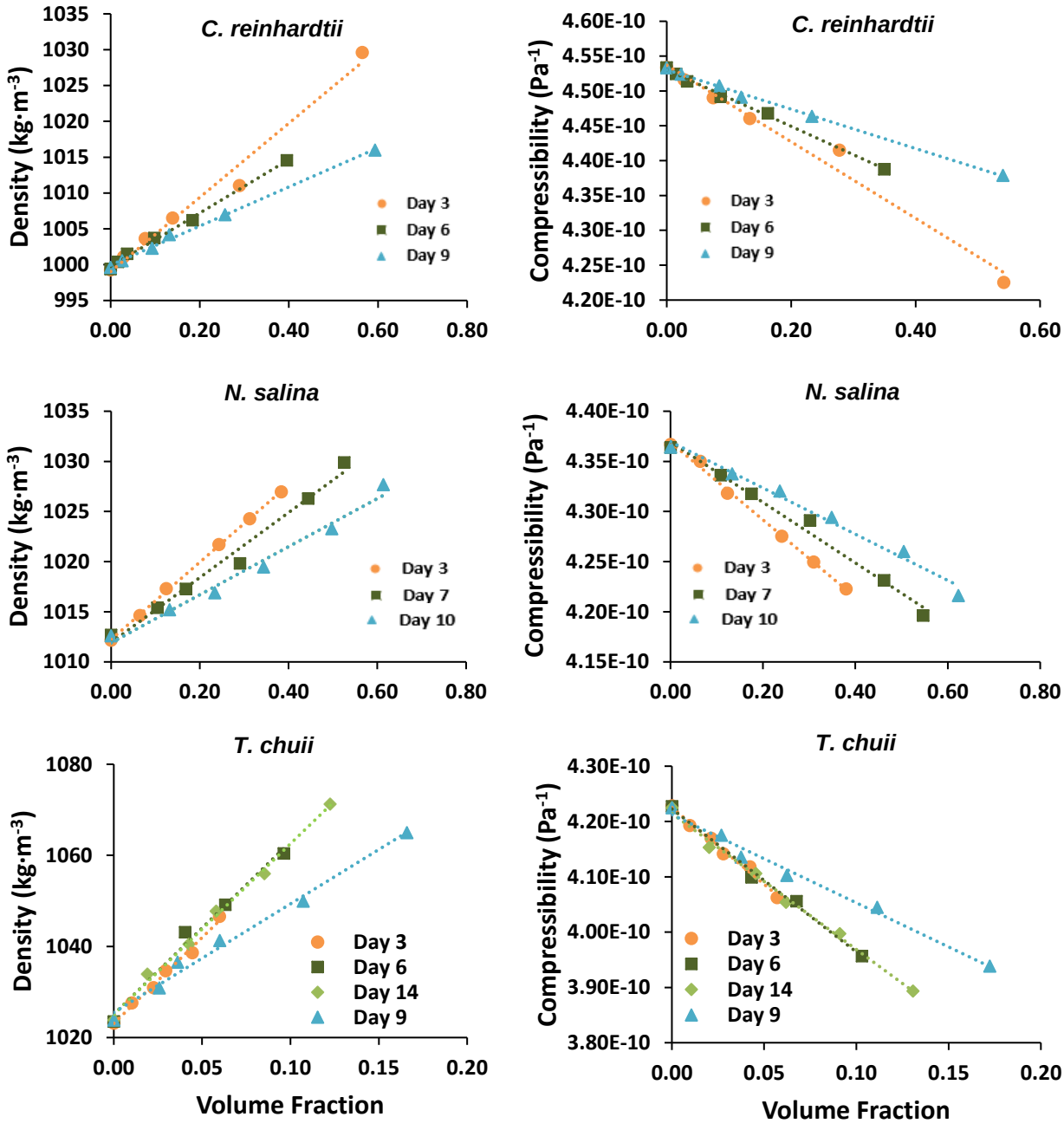

Figure 6. Density (left) and compressibility (right) of suspensions of *C. reinhardtii*, *N. salina*, and *T. chuii* in growth media as a function of the volume fraction of cells in the media on each acoustic measurement day.

Table 4. Variations in Cell size (average diameter, average cell volume, and diameter of average volume), cell properties (density and compressibility), and ACF of the cells in their respective growth media (property measurement approach and particle tracking approach) over the growth cycle for three microalgae strains. The uncertainty in the cell diameter is the standard deviation. For cell volume and diameter of average volume, the uncertainty is the 95% confidence interval on the mean. For cell density and compressibility the uncertainty is the standard deviation between each dilution sample. The uncertainty in the ACF represents the propagation of error due to the uncertainty in either average cell volume (for the property measurement approach) or cell diameter (for the particle tracking approach).

		Cell size			**Cell properties**		**ACF**	
Strain	**Day**	**Average diameter (μm)**	**Average volume (μm^3)**	**Dia. of average volume (μm)**	**Average density ($kg \cdot m^{-3}$)**	**Average compressibility (Pa^{-1})**	**Property measurement approach**	**Particle tracking approach**
C. reinhardtii	3	8.5 ± 1.5	335 ± 17	8.6 ± 0.2	1052 ± 8	$4.01 \times 10^{-10} \pm 6.96 \times 10^{-12}$	0.056 ± 0.003	0.040 ± 0.014
	6	8.0 ± 1.5	303 ± 13	8.3 ± 0.1	1047 ± 11	$4.09 \times 10^{-10} \pm 9.13 \times 10^{-12}$	0.048 ± 0.003	0.030 ± 0.011
	9	8.5 ± 1.0	353 ± 12	8.8 ± 0.1	1031 ± 4	$4.24 \pm\times 10^{-10}$ 4.07×10^{-12}	0.032 ± 0.001	0.020 ± 0.005
N. salina	3	4.3 ± 0.4	42 ± 2	4.3 ± 0.1	1051 ± 1	$4.01 \times 10^{-10} \pm 5.44 \times 10^{-12}$	0.040 ± 0.002	0.040 ± 0.008
	7	4.3 ± 0.4	40 ± 2	4.2 ± 0.1	1041 ± 3	$4.08 \times 10^{-10} \pm 2.70 \times 10^{-12}$	0.031 ± 0.002	0.030 ± 0.006
	10	4.3 ± 0.4	41 ± 2	4.3 ± 0.1	1033 ± 2	$4.16 \times 10^{-10} \pm 2.00 \times 10^{-12}$	0.023 ± 0.001	0.020 ± 0.004
T. chuii	3	12.5 ± 1.5	1075 ± 43	12.7 ± 0.2	1405 ± 36	$1.38 \times 10^{-10} \pm 3.76 \times 10^{-11}$	0.330 ± 0.014	0.330 ± 0.070
	6	11.0 ± 1.5	652 ± 34	10.8 ± 0.2	1448 ± 54	$1.33 \times 10^{-10} \pm 2.47 \times 10^{-11}$	0.339 ± 0.018	0.400 ± 0.105
	9	13.0 ± 2.0	1108 ± 64	12.8 ± 0.3	1306 ± 44	$2.26 \times 10^{-10} \pm 3.17 \times 10^{-11}$	0.235 ± 0.014	N/A
	14	11.5 ± 1.5	746 ± 31	11.3 ± 0.2	1444 ± 65	$1.24 \times 10^{-10} \pm 4.67 \times 10^{-11}$	0.357 ± 0.020	0.270 ± 0.065

The larger uncertainties in the ACF values for *T. chuii* is due to the larger diameter (~12 μm compared to 4.3 μm for *N. salina*) and greater variability in size (± 2 μm compared to 0.4 μm for *N. salina*) for those cells. These uncertainty values represent the propagation of error due to uncertainty in cell volume (and therefore volume fraction). A given uncertainty in diameter leads to greater uncertainty in volume for larger cells because volume is proportional to diameter

cubed. *N. salina* cells were smaller and more consistent in size, so the ACF estimate was more precise than for the other strains.

Although the ACFs of the strains investigated here approached zero as the growth cycle progressed and lipid content increased, none of the ACFs reached zero. Assuming the densities of lipids, proteins, and carbohydrates presented in Table 1, and assuming equal protein and carbohydrate contents, the lipid content required to reach an ACF of zero is estimated to be 93% from a theoretical perspective. Previous research by Hincapié Gómez et al. (2018) presented a case study showing that *Chlamydomonas reinhardtii* starch null sta6 mutant (CC-4348) cells transitioned from a positive to negative ACF [25]. The cells were cultivated in a phosphate-buffered high salt medium (HSM) with a nitrogen and acetate source [37]. Then the media was replaced by nitrogen-deprived HSM with 20mM acetate and the cells were boosted with 20mM acetate two days later as well [37]. At the beginning of the growth cycle, the cells migrated to the node of the acoustic wave, meaning that the ACF was positive [25]. In the middle of the growth cycle, the cells were unresponsive to the acoustic force and the ACF was zero [25]. At the end of the growth cycle, the cells accumulated such a high lipid content that they migrated to the antinode of the wave, meaning that the ACF was negative [25] [37]. After conducting the present research, it is expected that this special case of the ACF becoming zero and then negative is not common. The growth methods used on these *C. reinhardtii* (CC-4348) cells caused such a high lipid production that the cells were floating on water even when centrifuged [37]. Furthermore, this type of growth method is not widely used, if at all, in the microalgae biofuel and bioproducts industries.

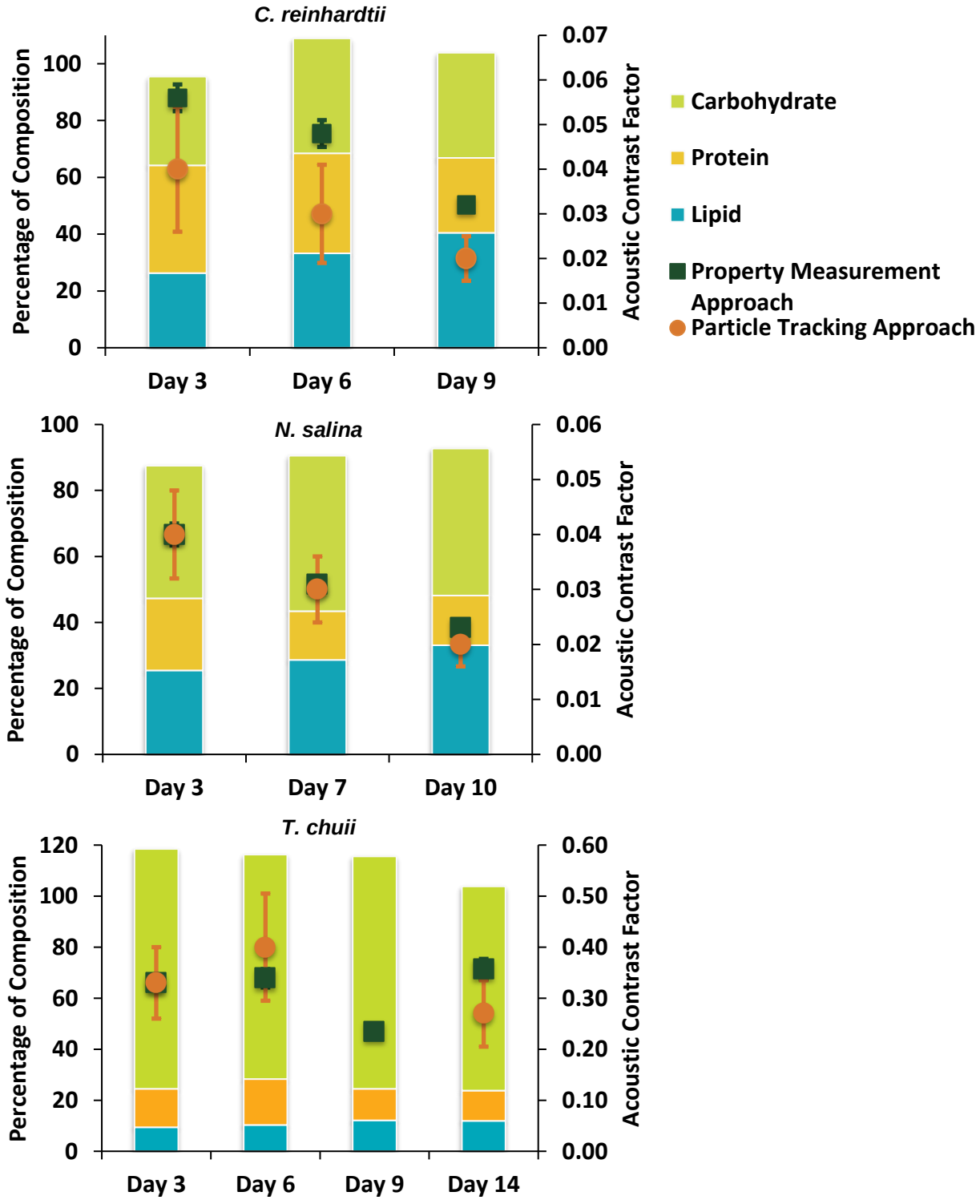

Figure 7. Cell composition as a function of acoustic measurement day is represented by the bar graphs and the left axis. ACF on each day, as determined by property measurement approach (green) and particle tracking approach (orange), is shown by the points and right axis. Error bars represent the propagation of the uncertainty in cell size. For *T. chuii*, the ACF for Day 9 was not calculated with the particle tracking approach.

3.1.3 Acoustic Contrast Factor Determined by the Particle Tracking Approach

The particle tracking approach involved recording videos of cell motion under the acoustic field and obtaining position versus time curves for three randomly selected cells. As illustrated in Figure 8, each cell (represented by the solid lines) started at a measured distance away from the node of the wave.

As time progressed, the cell moved toward the node due to the acoustic force. The shaded areas represent the COMSOL-predicted range of motion for a cell starting at that particular location, with the calculated acoustic contrast factor, based on the standard deviation in cell diameter. In some cases, such as for *N. salina* on day 10, the cells were moving too slow to reach the node within the length of the video. In other cases, the motion of a certain cell could not be tracked for the duration of the video because the cell moved behind other cells or off the edge of the video frame. These limitations do not impact the ability to calculate the ACF.

As shown in Table 4 and Figure 7, the ACF determined by the particle tracking approach decreased over time, similarly to the ACF calculated by the property measurement approach (Table 4). For both *C. reinhardtii* and *N. salina*, the ACF decreased by 50% over the growth cycle. For *T. chuii*, the ACF decreased by 18% over the 14-day growth period. The uncertainty for *T. chuii* was much greater due to the variability in its larger cell size. Based on the Tukey-Kramer method, the 18% decrease in ACF is not statistically significant.

For *C. reinhardtii*, the ACFs predicted by the particle tracking approach were systematically lower than the ACFs predicted by the property measurement approach. Based on the Tukey-Kramer method, the ACFs determined by the particle tracking approach were significantly different from the ACFs determined by the property measurement approach on days 3 and 6. Agreement between the two approaches was better for *N. salina* and *T. chuii*, with the

only significantly different ACF found on day 14 for *T. chuii*. It is expected that these differences between the two approaches are caused by the uncertainty in cell size.

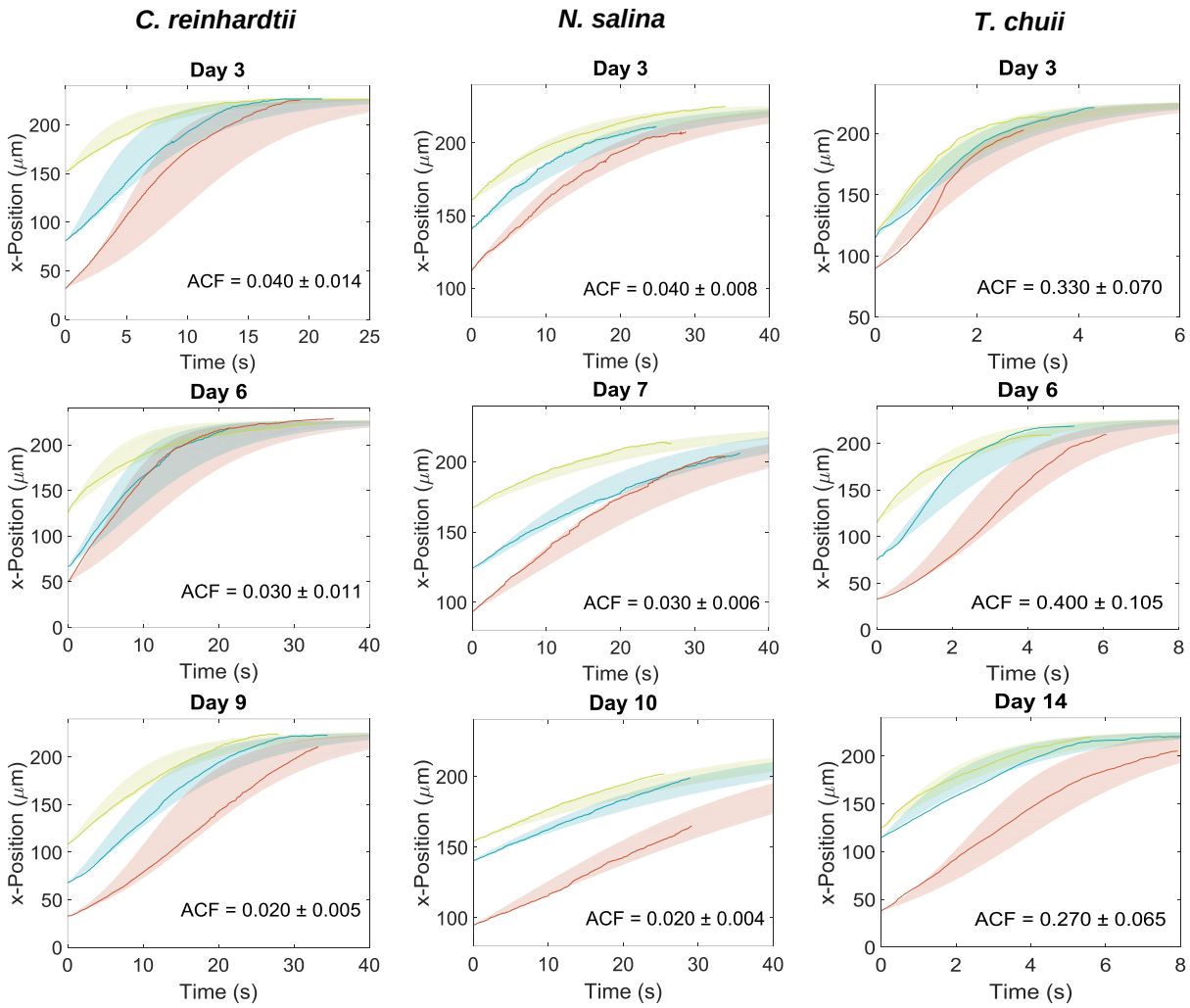

Figure 8. Motion of three randomly chosen *C. reinhardtii* (left), *N. salina* (middle), and *T. chuii* (right) cells on each acoustic measurement day measured using PTV in the solid lines. Shaded areas represent COMSOL modeling of where each cell should be with the range due to the standard deviation of the cell size on each day and the corresponding ACF.

The property measurement approach was easier and faster to complete. Additionally, this method was less susceptible to uncertainty in diameter since cell size was measured for large populations and the distributions were relatively narrow (Figure 9). The uncertainties associated with the particle tracking approach were larger than the uncertainties associated with the

property measurement approach. This is due to the larger uncertainty associated with the diameter of a single given cell (randomly chosen for tracking) than with the average cell diameter in a solution that contains millions of cells. Since the ACF is strongly dependent on diameter, there was more uncertainty with the former. However, the property measurement approach assumed that the cells behaved in such a way that they are homogenous (with a single density and compressibility). The particle tracking approach measured the actual motion of cells in an ultrasonic field, but it is not possible to determine the exact composition of those individual cells. With the current PTV setup it is not even possible to accurately determine the diameter of an individual cell. In the future, with better magnification, the diameter could be measured for each cell that is tracked. However, this approach will always require the use of bulk composition.

3.2 **Impact of Cell Size on Harvesting Performance**

In addition to the ACF, cell size greatly impacts the responsiveness of an algal species to ultrasonic harvesting. The two major properties of cells that affect their amenability to acoustic harvesting are cell size and acoustic contrast factor. In previous work, only 25 cells were measured to determine average volume [25]. In this study, 200-400 cells were measured. Additionally, cells in this study were measured at a higher magnification (20X and 40X instead of 10X), which generated higher-resolution images (i.e., more pixels per micron) and allowed for more accurate measurements. As seen in Figure 9, cell size did not vary much over the growth cycle. For *C. reinhardtii* and *T. chuii*, the bin size is 0.5 µm because these cells were measured using 20X magnification. For *N. salina*, the bin size is 0.1 µm because these smaller cells were measured at 40X magnification. Since *T. chuii* cells have a prolate spheroid shape, the effective diameters are shown in Figure 9.

Due to the relationship between the acoustic radiation force and drag force described in Section 1.2, the theoretical net force acting on cells in an acoustic harvesting system is proportional to Φa^2. Although the change in ACF (due to changes in cellular composition) over the course of a growth cycle is expected to affect the effectiveness of acoustic harvesting (Figure 7), cell size has a much greater impact on magnitude of the net force than cellular composition. In Figure 10, the ACF multiplied by the cell radius squared (Φa^2) is shown over each algal species' growth cycle. The relative difference in Φa^2 between each species is largely due to differences in cell size. The 50× higher Φa^2 value associated with *T. chuii*, compared to *N. salina*, is largely due to *T. chuii* cells having a diameter that is 3× the diameter of *N. salina* cells. However, differences in cellular composition also contribute: *T. chuii* contained roughly one third of the amount of lipids compared to *C. reinhardtii* and *N. salina*. Since *T. chuii* was composed of almost entirely carbohydrates (Table 3), the ACF of *T. chuii* was approximately an order of magnitude higher than that of the other algal strains in this study.

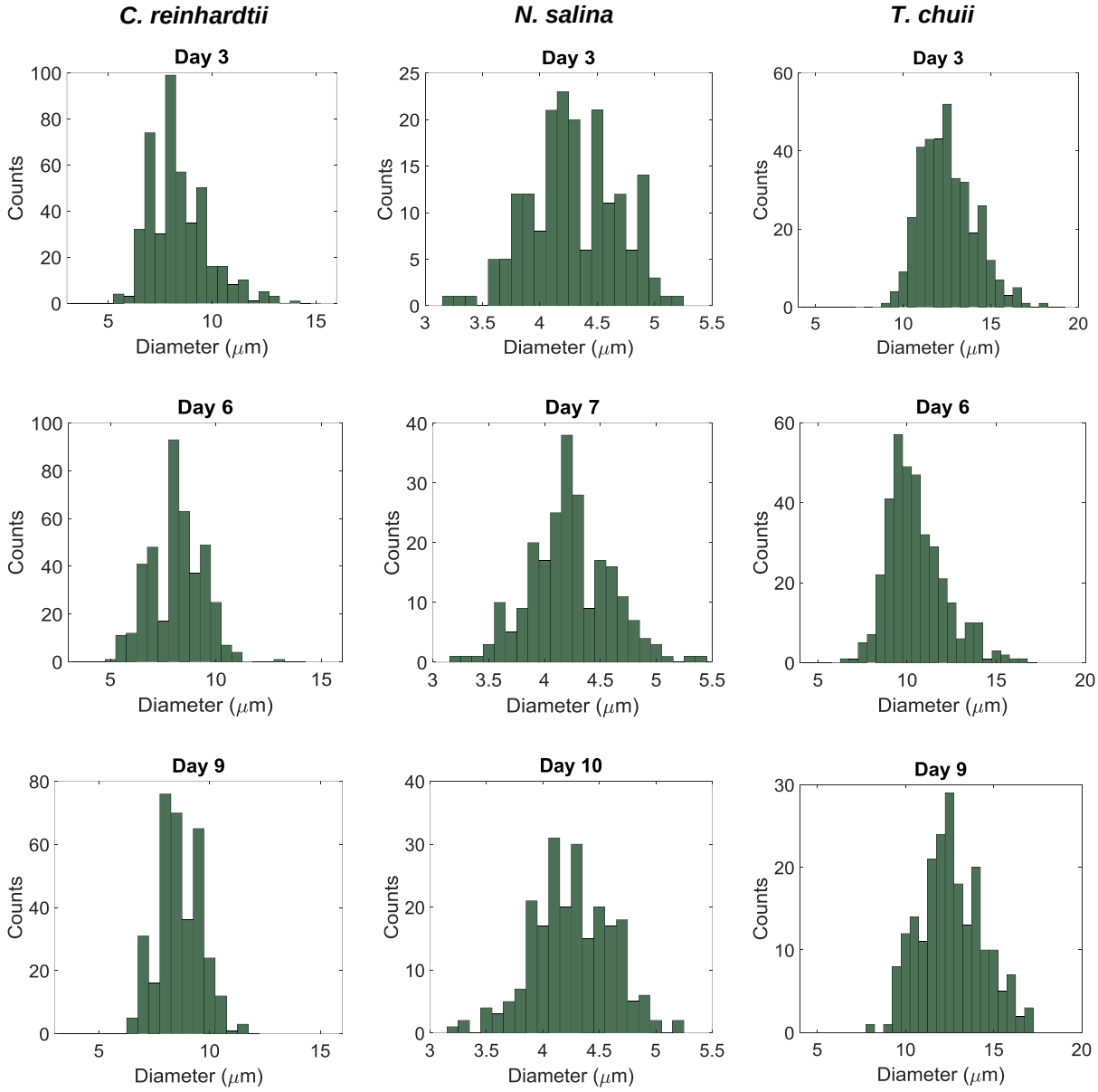

Figure 9. Histogram of cell size for *C. reinhardtii* (left), *N. salina* (middle), and *T. chuii* (right) on each acoustic measurement day. The average diameter for *C. reinhardtii* was 8.5 µm, 8.0 µm, and 8.5 µm on day 3, 6, and 9, respectively. For *N. salina*, the average diameter on each day was 4.3 µm. For *T. chuii*, the average effective diameter was 12.5 µm, 11.0 µm, and 13.0 µm, and 11.5 µm on Day 3, 6, 9, and 14, respectively. The histogram for day 14 can be found in Appendix I.

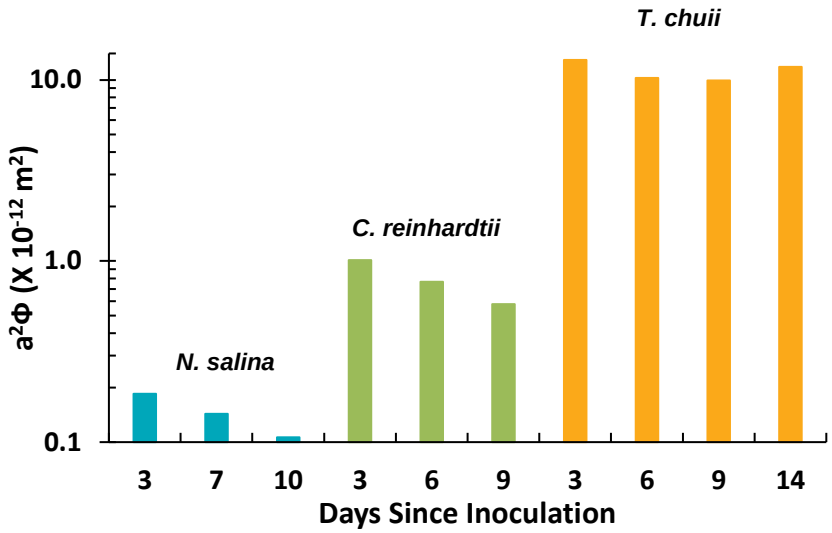

Figure 10. Acoustic contrast factor (property measurement approach) multiplied by the effective cell radius squared ($a^2\Phi$) over the growth cycle for each algal strain. This metric is proportional to the ratio of the acoustic radiation force to the drag force. Blue bars represent *N. salina*, green bars represent *C. reinhardtii*, and orange bars represent *T. chuii*. The y-axis is on a log 10 scale.

4 CONCLUSION

This research investigated the change in acoustic properties over a 2-week growth period for three algal strains: *C. reinhardtii*, *N. salina,* and *T. chuii*. These three algal strains have been utilized in the biofuels and bioproducts industries [58] [59] [60]. Furthermore, their cell composition was in agreement with those found in the literature [55] [56] [57]. As lipids accumulated in *C. reinhardtii* and *N. salina* over their growth periods, the ACF of the cells approached zero but did not become zero. For *C. reinhardtii* the lipid content increased from 26% ± 1% to 40% ± 1% from day 3 to 9, which resulted in a 43% decrease in ACF (0.056 ± 0.003 to 0.032 ± 0.001). For *N. salina* the lipid content increased from 25% ± 1% to 33% ± 1% from day 3 to 10, which also resulted in a 43% decrease in ACF (0.040 ± 0.002 to 0.023 ± 0.001). For *T. chuii* the lipid content remained relatively stable throughout the growth period so the ACF did not change significantly. Acoustic harvesting is rendered ineffective when the ACF is equal to zero. Since the ACF remained nonzero over each strains growth period, this proved that the cells would still be responsive to the acoustic force. Therefore, ultrasonic harvesting could be utilized throughout the growth cycle. However, the cell composition and resulting ACF should be considered at the point in the growth cycle when harvesting will occur.

Two methods were used to determine the ACF of algal cells: 1) property measurement approach and 2) particle tracking approach. Benefits for the property measurement approach include quicker and easier experiments and reduced uncertainty with cell variation because this method relies on bulk measurements. Conversely, the particle tracking approach determines the motion of individual particles to calculate the ACF. This could be viewed as a drawback since only a limited number of cells can be measured. However, this method determines the response

of cells under the acoustic force and drag force and shows the variation of non-homogeneous cells. This research has shown that both approaches are reliable methods to determine the ACF.

In addition to cell composition, the size of the cells impacts the responsiveness of an algal strain to acoustic harvesting. Since the net force acting on the cells is proportional to Φa^2, the size of the cell is arguably more important than the composition (for cells with nonzero ACF's). Figure 10 highlights this hypothesis as Φa^2 between species is much larger than Φa^2 over the growth period of one species. With the goal to maximize Φa^2 to improve ultrasonic harvesting efficiency, the most compatible cells for ultrasonic harvesting would be low in lipid content and large in size. This suggests that acoustic harvesting would work well with algae used for hydrothermal liquefaction conversion to biofuels because high lipid content is not required for this technique. This low-energy harvesting technology has the potential to provide a cost-effective solution to harvesting microalgae when paired with a compatible species. Future work is necessary to design a scalable ultrasonic harvester that could meet the needs of the microalgae industry.

REFERENCES

[1] J. A. Church and N. J. White, "A 20th Centruy Acceleration in Global Sea-level Rise," *Geophysical Research Letters,* vol. 33, no. 1, 2006.

[2] U.S. Global Change Research Program, "Global climate change impacts in the United States: A state of knowledge report," Cambridge UP, 2009.

[3] P. Fairley, "Introduction: next generation biofuels," *Nature,* vol. 474, no. dx.dio.org/10.1038/474S02a, pp. S2-S5, 2011.

[4] DOE, "National Algal Biofuels Technology Review," U.S. Department of Energy Office of Energy Efficiency and Renewable Energy, 2016.

[5] U.S. Government, "Energy Independence and Security Act of 2007," 2007.

[6] K. Bracmort, "Algae's Potential as a Transportation Biofuel," Congressional Research Service, Washington, DC, 2013.

[7] R. Schnepf and B. D. Yacobucci, "Renewable Fuel Standard (RFS): Overview and Issues," Congressional Research Service, Washington, DC, 2013.

[8] A. Demirbas and M. F. Demirbas, "Importance of algae oil as a source of biodiesel," *Energy Conversion and Management,* vol. 52, no. 1, pp. 163-170, 2011.

[9] Y. Chisti, "Biodiesel from microalgae beats bioethanol," *Trends in Biotechnology,* vol. 26, no. 3, pp. 126-131, 2008.

[10] A. Singh, P. Singh Nigam and J. D. Murphy, "Renewable fuels from algae: an answer to debatable land based fuels," *Bioresource Technology,* vol. 102, no. 1, pp. 10-16, 2011.

[11] J. C. Quinn, K. Catton, N. Wagner and T. H. Bradley, "Current large-scale US biofuel potential from microalgae cultivated in photobioreactors," *BioEnergy Res.,* vol. 5, pp. 49-60, 2012.

[12] B. Wang, Y. Li, N. Wu and C. Q. Lan, "CO2 Bio-Mitigation Using Microalgae," *Applied Microbiology and Biotechnology,* vol. 79, no. 5, pp. 707-718, 2008.

[13] P. T. Pienkos and A. Darzins, "The promise and challenges of microalgal-derived biofuels," *Biofuels Bioprod. Biorefin.,* vol. 19, pp. 431-440, 2009.

[14] J. Fabregas and C. Herrero, "Marine microalge as a potential source of single cell protein," *Applied Microbiology and Biotechnology,* vol. 23, no. 2, pp. 110-113, 1985.

[15] M. A. Borowitzka, "High-value products from microalgae-their development and commercialisation," *Journal of Applied Phycology,* vol. 25, no. 3, pp. 743-756, 2013.

[16] J. C. Quinn and R. Davis, "The potentials and challenges of algae based biofuels: a reivew of the techno-economic, life cycle, and resource assessment modeling," *Bioresource Technology,* vol. 184, pp. 444-452, 2015.

[17] K. Pirwitz, R. J. Flassig, L. Rihko-Struckmann and K. Sundmacher, "Energy and operating cost assessment of competing harvesting methods for D. salina in a β-carotene production process," *Algal Research,* vol. 12, pp. 161-169, 2015.

[18] K. Sander and G. S. Murthy, "Life cycle analysis of algae biodiesel," *The International Journal of Lice Cycle Assessment,* vol. 15, no. 7, pp. 440-449, 2010.

[19] N. V. Baker, "Segregation and sedimentation of red blood cells in ultrasonic standing waves," *Nature,* vol. 239, pp. 398-399, 1972.

[20] T. Ryll, G. Dutina, A. Reyes, J. Gunson, L. Krummen and T. Etcheverry, "Performance of small-scale CHO perfusion cultures using an acoustic cell filtration device for cell retention: characterization of separation efficiency and impact of perfusion on product quality," *Biotechnology and Bioengineering,* vol. 69, no. 4, pp. 440-449, 2000.

[21] J. Dionne, B. Mccarthy, B. Ross-Johnsrud, L. Masi and B. Lipkens, "Large volume flow rate acoustophoretic phase separator for oil water emulsion splitting," *The Journal of the Acoustical Society of America,* vol. 133, 2013.

[22] P. Juliano, M. A. Augustin, X.-Q. Xu, R. Mawson and K. Knoerzer, "Advances in high frequency ultrasound separation of particulates from biomass," *Ultrasonics Sonochemistry,* vol. 35, pp. 577-590, 2017.

[23] R. Bosma, W. A. van Spronsen, J. Tramper and R. H. Wijffels, "Ultrasound, a new separation technique to harvest microalgae," *Journal of Applied Phycology,* vol. 15, pp. 143-153, 2003.

[24] J. E. Coons, D. M. Kalb, T. Dale and B. I. Marrone, "Getting to low-cost algal biofuels: a monograph on conventional and cutting-edge harvesting and extraction technologies," *Algal Research,* vol. 6, pp. 250-270, 2014.

[25] E. Hincapié Gómez, J. Tryner, A. J. Aligata, J. C. Quinn and A. Marchese, "Measurement of acoustic properties of microalgae and implications for the," *Algal Research,* vol. 31, pp. 77-86. doi.org/10.1016/j.algal.2018.01.015, 2018.

[26] J. Blauert and N. Xiang, Acoustics for Engineers: Troy Lectures, Springer, 2009.

[27] F. Jacobsen, Fundamentals of general linear acoustics, Wiley, 2013.

[28] L. Yang and L. Kian-Meng, "Particle separation in microfluidics using switching ultrasonic field," *Lab on a Chip,* pp. 3167-3173, 2011.

[29] K. Yoshioka and Y. Kawashima, "Acoustic radiation pressure on a compressible sphere," *Acoustica,* vol. 5, no. 3, pp. 167-173, 1955.

[30] H. Bruus, "Acoustofluidics 7: The acoustic radiation force on small particles," *Lab on a Chip,* vol. 12, no. 1014. doi:10.1039/c2lc21068a, 2012.

[31] S. Gupta, D. L. Feke and I. Manas-Zloczower, "Fractionation of mixed particulate solids according to compressibility using ultrasonic standing wave fields," *Chemical Engineering Science,* vol. 50, no. 20, pp. 3275-3284, 1995.

[32] M. Gröschl, "Ultrasonic separation of sustpended particles - part I: fundamentals," *Acta Acoustica,* vol. 84, no. 3, pp. 432-447, 1998.

[33] B. L. Johnson, M. R. Holland, J. G. Miller and J. I. Katz, "Ultrasonic attenuation and speed of sound of cornstarch suspensions," *J. Acoust. Soc. Am.,* vol. 133, pp. 1399-1403, 2013.

[34] B. Gavish, E. Gratton and C. J. Hardy, "Adiabatic compressibility of globular proteins," *Proc. Natl. Acad. Sci.,* vol. 80, pp. 750-754, 1983.

[35] T. N. Pashovkin and D. G. Sadikova, "Cell exfloliation, separation, and concentration in the field of a standing ultrasonic wave," *Acoust. Phys.,* vol. 55, pp. 584-593, 2009.

[36] Dantec Dynamics, "PSP, HGS, S-HGS, and FPP Seeding Materials," [Online]. Available: https://www.dantecdynamics.com/seeding-materials. [Accessed 4 August 2017].

[37] C. Goodson, R. Roth, Z. T. Wang and U. Goodenough, "Structural correlates of cytoplasmic and chloroplast lipid body synthesis in Chlamydomonas Reinhardtii and stimulation of lipid body production with acetate boost," *Eukaryot. Cel,* vol. 10, pp. 1592-1606, 2011.

[38] U. Goodenough, I. Blaby, D. Casero, S. D. Gallaher, C. Goodson, S. Johnson, J. H. Lee, S. S. Merchant, M. Pellegrini, R. Roth, J. Rusch, M. Singh, J. G. Umen, T. L. Weiss and T. Wulan, "The path to Triacylglyceride obesity in the sta6 strain of Chlamydomonas Reinhardtii," *Eukaryot. Cell,* vol. 13, pp. 591-613, 2014.

[39] K. Napan, D. Hess, B. McNeil and J. C. Quinn, "Quantification of Heavy Metals and Other Inorganic Contaminants on the Productivity of Microalgae," *J Vis Exp.,* no. 101. doi: 10.3791/52936, 2015.

[40] C. J. Zhu and Y. K. Lee, "Determination of biomass dry weight of marine microalgae," *Journal of Applied Phycology,* vol. 9, pp. 189-194, 1997.

[41] R. Peck, C. Olsen and J. Devore, Introduction to Statistics and Data Analysis, 3rd ed., Belmont, CA: Brooks/Cole, 2009.

[42] S. K. Mishra, W. I. Suh, W. Farooq, M. Moon, A. Shrivastav, M. S. Park and J.-W. Yang, "Rapid quantification of microalgal lipids in aqueous medium by a simple colorimetric method," *Bioresource Technology,* vol. 155, no. doi: 10.1016/j.biortech.2013.12.077, pp. 330-333, 2014.

[43] O. H. Lowry, N. J. Rosebrough, A. L. Farr and R. J. Randall, "Protein measurement with the Folin phenol reagent," *Journal of Biological Chemistry,* vol. 193, pp. 265-275, 1951.

[44] C. V. González López, M. d. C. C. García, F. G. A. Fernández, C. Segovia Bustos, Y. Chisti and J. M. Fernández Sevilla, "Protein measurements of microalgal and cyanobacterial biomass," *Bioresource Technology,* vol. 101, no. doi.org/10.1016/j.biortech.2010.04.077, pp. 7587-7591, 2010.

[45] G. L. Peterson, "Review of the Folin phenol protein quantification method of Lowry, Rosebrough, Farr and Randall," *Analytical Biochemistry,* vol. 100, pp. 201-220, 1979.

[46] A. A. Albalasmeh, A. A. Berhe and T. A. Ghezzehei, "A new method for rapid determination of carbohydrate and total carbon concentrations using UV spectrophotometry," *Carbohydrate Polymers,* vol. 97, pp. 253-261, 2013.

[47] M. DuBois, K. Gilles, J. Hamilton, P. Rebers and F. Smitch, "Colorimetric method for determination of sugars and related substances," *Analytical Chemistry,* vol. 28, no. 3, pp. 350-356, 1956.

[48] L. M. L. Laurens, T. A. Dempster, H. D. T. Jones, E. J. Wolfrum, S. Van Wychen, J. S. P. McAllister, M. Renecenberger, K. J. Parchert and L. M. Gloe, "Algal biomass constituent analysis: method uncertainties and investigation of the underlying measuring chemistries," *Analytical Chemistry,* vol. 84, no. 4, pp. 1879-1887, 2012.

[49] S. Van Wychen and L. M. L. Laurens, "Determination of total solids and ash in algal biomass," National Renewable Energy Laboratory, Golden, CO, 2013.

[50] P. Biller and A. B. Ross, "Potential yields and properties of oil from the hydrothermal liquefaction of microalgae with different biochemical content," *Bioresource Technology,* vol. 102, pp. 215-225, 2011.

[51] P. J. Hansen, "Use of a Hemacytometer," University of Florida Department of Animal Sciences, Gainesville, FL, 2000.

[52] H. Hillebrand, C. D. Dürselen, D. Kirschtel, U. Pollingher and T. Zohary, "Biovolume Calculation for Pelagic and Benthic Microalgae," *Journal of Phycology,* vol. 35, no. doi:10.1046/j.1529-8817.1999.3520403.x, pp. 403-424, 1999.

[53] R. J. Urick, "A sound velocity method for determining the compressibility of," *J. Appl. Phys.,* vol. 18, no. http://dx.doi.org/10.1063/1.1697584, pp. 983-987, 1947.

[54] S. K. Gupta, A. Malik and F. Bux, Algal Biofuels: Recent Advances and Future Prospects, Springer, 2017.

[55] M. R. Brown, "The amino-acid and sugar composition of 16 species of microalgae used in mariculture," *Journal of Experimental Marine Biology and Ecology,* vol. 145, no. 1, pp. 79-99, 1991.

[56] S. Yu, Q. Zhao, X. Miao and J. Shi, "Enhancement of lipid production in low-starch mutants Chlamydomonas reinhardtii by adaptive laboratory evolution," *Bioresource Technology,* vol. 147, pp. 499-507, 2013.

[57] D. Hess, K. Napan, B. T. McNiel, E. M. Torres, T. Guy, J. E. McLean and J. C. Quinn, "Quantification of effects of flue gas derived inorganic contaminants on microalgae growth system and end fate of contaminants," *Algal Research,* vol. 25, pp. 68-75, 2017.

[58] M. J. Griffiths and S. T. L. Harrison, "Lipid productivity as a key characteristic for choosing algal species for biodiesel production," *Journal of Applied Phycology,* vol. 21, pp. 493-507, 2009.

[59] Q. Hu, M. Sommerfeld, E. Jarvis, M. Ghirardi, M. Posewitz, M. Seibert and A. Darzins, "Microalgal triacylglycerols as feedstocks for biofuel production: perspectives and advances," *Plant J.*, vol. 54, pp. 621-639, 2008.

[60] M. L. Bartley, W. J. Boeing, B. N. Dungan, F. O. Holguin and T. Schaub, "pH effects on growth and lipid accumulation of the biofuel microalgae Nannochloropsis salina and invading organisms," *Journal of Applied Phycology*, pp. 1431-1437, 2014.

[61] R. A. Dulley and P. A. Grieve, "A simple technique for eliminating interference by detergents in the Lowry method of protein determination," *Analytical Chemistry*, vol. 64, pp. 136-141, 1975.

[62] M. B. Lees and S. Paxman, "Modification of the Lowry procedure for the analysis of proteolipid protein," *Analytical Biochemsitry*, vol. 47, pp. 184-192, 1972.

[63] D. J. Murphy and R. T. Prinsley, "Interaction of Triton X-100 with the pigment-protein complexes of photosynthetic membranes," *Biochemistry Journal*, vol. 229, pp. 31-37, 1985.

[64] W. J. Hurkman and C. K. Tanaka, "Solubilization of plant membrane proteins for analysis by two-dimensional gel electrophoresis," *Plant Physiology*, vol. 81, pp. 802-806, 1986.

[65] G. C. Dismukes, D. Carrieri, N. Bennette, G. M. Ananyev and M. C. Posewitz, "Aquatic phototrophs: efficient alteratives to land-based crops for biofuels," *Curr. Opin. Biotechnol.*, vol. 19, pp. 235-240, 2008.

[66] K. M. Weyer, D. R. Bush, A. Darzins and B. D. Willson, "Theoretical maximum algal oil production," *BioEnergy Res.*, vol. 3, pp. 204-213, 2010.

[67] DOE, "National Algal Biofuels Technology Roadmap," U.S. Department of Energy, Office of Energy Efficiency and Renewable Energy, Washington, DC, 2010.

[68] N. Uduman, Y. Qi, M. K. Danquah, G. M. Forde and A. Hoadley, "Dewatering of microalgal cultures: a major bottleneck to algae-based fuels," *Journal of Renewable Sustainable Energy*, vol. 2, p. 012701, 2010.

[69] J. J. Milledge and S. Heaven, "A review of the harvesting of micro-algae for biofuel production," *Rev. Environ. Sci. Biotechnol.*, vol. 12, pp. 165-178, 2013.

[70] ANL, NREL and PNNL, "Renewable Diesel from Algal Lipids: An Integrated Baseline for Cost, Emissions, and Resource Potential from a Harmonized Model," Argonne National Laboratory; National Renewable Energy Laboratory; Pacific Northwest National Laboratory, Argonne, IL; Golden, CO; Richland, WA, 2012.

[71] E. Hincapié Gómez and A. J. Marchese, "An ultrasonically enhanced inclined settler for microalgae harvesting," *Biotechnology Progress*, vol. 31, pp. 414-423, 2015.

[72] J. A. Olivares, I. Baxter, J. Brown, M. Carleton, R. A. Cattolico, D. Taraka, J. C. Detter, T. P. Devarenne, S. K. Dutcher, D. T. Fox, U. Goodenough, J. Jaworski, D. Kramer, M. S. Lipton, M. McCormick, S. Merchant, I. Molnar, E. A. Panisko, M. Pellegrini, J. Polle, M. Sabarsky, R. T. Sayre, Starkenburg, G. Stormo, S. N. Twary, C. J. Unkefer, J. S. Yuan, B. Arnold, X. Bai, W. Boeing, L. Brown, N. Gujarathi, M. Huesemann, P. Lammers, P. Laur, N. Khandan, R. Parsons, T. Samocha, A. Thomasson, A. Unc, P. Waller, J. Bonner, J. Coons, S. Fernando, B. Goodall, K. Kadam, R. Lacey, L. Wei, B. Marrone, Z. Nikolov, Trewyn B., K. Albrecht, S. Capareda, S. Cheny, S. Deng, D. Elliot, G. Cesar, R. Hallen, S. Lupton, S. Lynch, A. Marchese, J. Nieweg, K. Ogden, J. Oyler, K. Reardon, W. Roberts, D. Sams, T. Schaub, P. Silks, S. Archibeque, J. Foster, D. Gaitlan, A. Lawrence, S. Lodge-Ivey, T. Wickersham, P. Blowers, R. Davis, C. M. Downes, E. Dunlop, E. Frank, R. Handler, D. Newby, P. Pienkos, J. Richardson, W. Seider, D. Shonnard and R. Skaggs, "National Alliance for Advanced Biofuels and Bio-Products Final Technial Report," Donald Danforth Plant Science Center, St. Lois, MO, 2014.

[73] Q. Hu, M. Sommerfeld, E. Jarvis, M. Ghirardi, M. Posewitz, M. Seibert and A. Darzins, "Microalgal triacylglycerols as feedstocks for biofuel production: perspectives and advances," *The Plant Journal*, vol. 54, pp. 621-639, 2008.

APPENDIX I

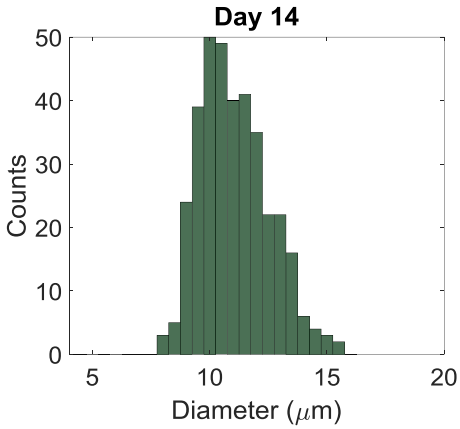

Figure 11. Histogram of cell size *T. chuii* on Day 14. The average effective diameter is 11.5 µm.